# Ultracompact Optical Fiber Sensor for Refractive Index and High-Temperature Measurement

C. R. Liao, H. F. Chen, and D. N. Wang, *Senior Member, IEEE*

***Abstract*—An ultracompact microfiber sensor head is demonstrated for refractive index and high temperature sensing. Such a device is a fiber in-line Mach–Zehnder interferometer formed by creating an inner air-cavity along a section of microfiber and exhibits a high refractive index sensitivity of ~4202 nm/refractive index unit and a good temperature sensitivity of 41 pm/°C, with excellent high-temperature sustainability up to 1100 °C.**

***Index Terms*—Femtosecond (fs) laser ablation, optical fiber interferometer, optical fiber sensors.**

## I. Introduction

TO COPE with the rapid development of optical fiber sensor network, sensor heads that exhibit ultra compact size and good capability of performing multiple sensing functions with high sensitivity are critically important. One promising candidate of such sensor heads is fiber in-line interferometer, which has been used in a wide range of sensing applications with various configurations [1]–[19]. In recent years, optical fiber in-line Mach–Zehnder interferometer (MZI) based on open air-cavity has been developed, which has large refractive index (RI) difference between the fiber core and air and hence high sensitivity while exhibiting a compact sensor head with length of only a few 100s $\mu$m or less [13], [14]. Such a device has high sensitivities for RI and temperature sensing and excellent high temperature sustainability thus being suitable for many chemical, biological, and environmental monitoring applications. However, most of the sensor heads are still limited by the single mode fiber (SMF) diameter of 125 $\mu$m. An effective way to reduce the optical fiber diameter and further improve the sensor head compactness is to use microfiber [20]–[24]. Because of its small diameter of down to micrometer order and large evanescent field for the guided light, microfiber activates strong interaction between the propagating light and the external environment, which makes it a highly sensitive element to the surrounding medium.

In this paper, an ultra compact microfiber sensor head based on inner air-cavity is presented for RI and high temperature sensing. The sensor head has a diameter of a few 10s $\mu$m and length of a few 100s $\mu$m and the sensitivities achieved for RI and temperature are ~4202 nm/refractive index unit (RIU) and 41 pm/ °C, respectively, with excellent high temperature sustainability up to 1100 °C.

## II. Device Fabrication

The optical fiber sensor head is fabricated by using femtosecond (fs) laser micromachining, fusion splicing, and heating and pulling techniques.

During the fabrication process, a Ti: sapphire laser system consisting of an oscillator (Mai Tai) and an amplifier (Spitfire), with pulse duration of 120 fs, repetition rate of 1 kHz, and operation wavelength of 800 nm was used. The laser pulses were focused onto the fiber by a 20X objective lens with an NA value of 0.5. A section of SMF (SMF-28 from Corning) with the core diameter of 8.2 $\mu$m and the nominal effective index of 1.4682 (at 1550 nm) was mounted on a computer controlled X-Y-Z translation stage with a 40-nm resolution. The steps of fabrication are illustrated in Fig. 1.

1) A micro-hole of several micrometers in diameter at the center of the cleaved fiber end facet was ablated by use of fs laser with the on-target laser power of ~5 mW. The micro-hole size determines the size and shape of the hollow sphere and hence the air-cavity formed later.
2) The fiber tip with the micro-hole structure was spliced together with another cleaved SMF tip by use of fusion splicer with fusing current of ~16.3 mA and fusing duration of ~2.0 s. The two splicing parameters also play an important role in determining the size and the shape of the air-cavity in microfiber formed later.
3) Since the air in the hole was suddenly heated, the hole rapidly expanded to an elliptical hollow sphere.
4) The SMF with hollow sphere was mounted between two translation stages and drawn into microfiber by use of flame brushing technique, i.e., to use a small flame moving under an optical fiber that was being stretched. By appropriately control the moving speed of the flame and the holders, microfiber of different diameters could be produced, with an inner air-cavity along the fiber length.

Manuscript received February 26, 2014; revised May 7, 2014 and May 26, 2014; accepted May 29, 2014. Date of publication June 5, 2014; date of current version July 2, 2014. This project is supported by the National Natural Science Foundation of China (Grant No. 61377094) and also by the Hong Kong Polytechnic University research grants 4-ZZE3.

C. R. Liao is with the College of Optical and Electronic Technology, China Jiliang University, Hangzhou, 310018, China and Department of Electrical Engineering, The Hong Kong Polytechnic University, Kowloon, Hong Kong, and also with the Key Laboratory of Optoelectronic Devices and Systems of Ministry of Education and Guangdong Province, College of Optoelectronic Engineering, Shenzhen University, Shenzhen, 518060, China.

H. F. Chen is with the College of Optical and Electronic Technology, China Jiliang University, Hangzhou, 310018, China and Department of Electrical Engineering, The Hong Kong Polytechnic University, Kowloon, Hong Kong, and also with the State Key Laboratory of Modern Optical Instrumentations, Zhejiang University, Hangzhou, 310027, China.

D. N. Wang is with the College of Optical and Electronic Technology, China Jiliang University, Hangzhou, 310018, China and Department of Electrical Engineering, The Hong Kong Polytechnic University, Kowloon, Hong Kong, and also with the Hong Kong Polytechnic University Shenzhen Research Institute, Shenzhen 518057, China, and School of Electrical, Electronic and Information Engineering, Hubei Polytechnic University, Huangshi, China (e-mail: eednwang@polyu.edu.hk).

Color versions of one or more of the figures in this paper are available online at http://ieeexplore.ieee.org.

Digital Object Identifier 10.1109/JLT.2014.2328356

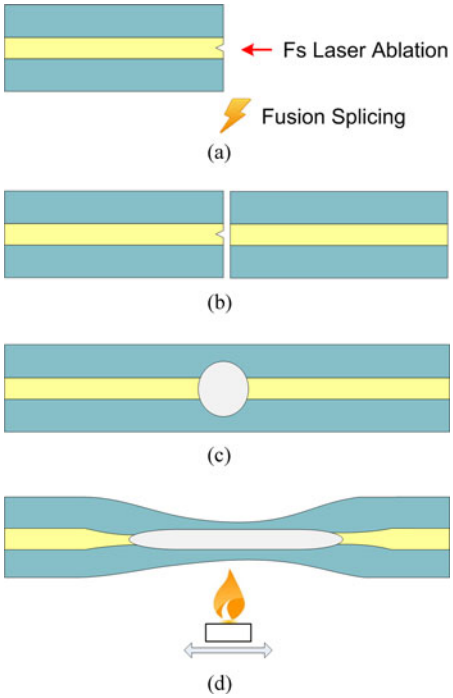


Fig. 1. Schematic diagram of fabrication process of the microfiber with inner air-cavity. (a) Micro- hole ablated by fs laser. (b) The fiber tip with micro-hole spliced together with another cleaved SMF tip. (c) Hollow sphere formed in SMF. (d) Device produced by brushing technique.

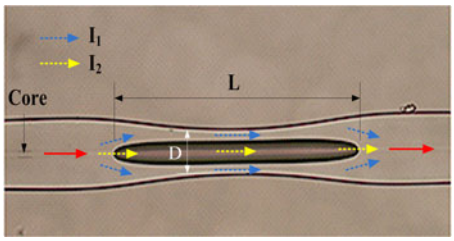


Fig. 2. (Color online) Schematic diagram of the sensor.

## III. Principle of Operation

The schematic diagram of the sensor head is illustrated in Fig. 2. The light lunched into the inner air-cavity is split into two beams: one travels along the silica wall of the cavity, which is denoted by $I_1$; and the other passes through the air-cavity, denoted by $I_2$. The interference takes place when the two beams recombine at the cavity end. The output intensity of the MZI is governed by [24]

$$I = I_1 + I_2 + 2\sqrt{I_1 I_2}\cos\left(\frac{2\pi L\Delta n}{\lambda}\right) \tag{1}$$

where $I$ represents the intensity of the interference signal, $\lambda$ is the wavelength, $L$ is the cavity length, $\Delta n = n_{\text{wall}} - n_{\text{cavity}}$ denotes the effective RI difference of the two interference beams, $n_{\text{wall}}$ and $n_{\text{cavity}}$ are the effective RI of the silica wall mode and the air-cavity mode, respectively. Compared with the conventional microfiber of similar size, the thinner cavity wall leads to a large evanescent field in one arm of the MZI,

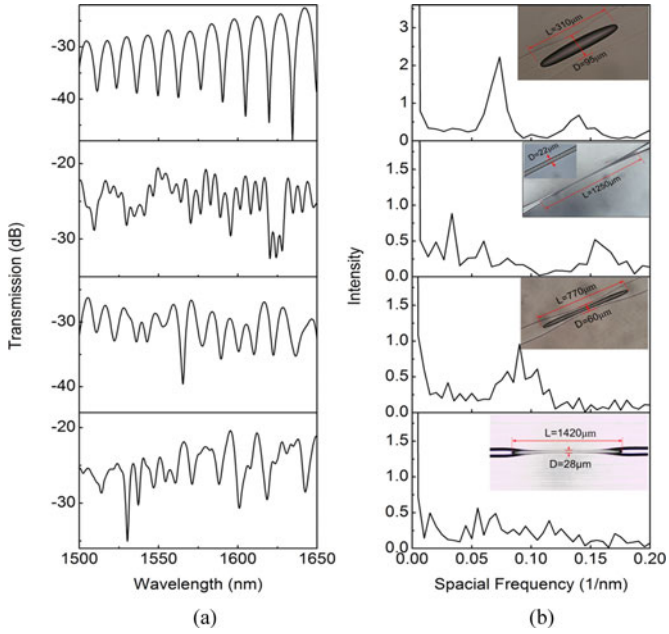


Fig. 3. (Color online) (a) Transmission spectra of the device samples. (b) Spatial frequency spectra of the device samples, and the insets show their microscope images.

and hence, the enhanced light interaction with the surrounding medium is expected. When the phase term satisfies the condition $2\pi L\Delta n/\lambda = (2m+1)\pi$, where $m$ is an integer, the intensity dip appears at the wavelength

$$\lambda_{\text{dip}} = \frac{2L\Delta n}{2m+1}. \tag{2}$$

Thus, the free spectral range (FSR) of the spectrum can be expressed as

$$\text{FSR} = \frac{\lambda^2}{\Delta n L}. \tag{3}$$

## IV. Experimental Results and Discussion

To test microfiber in-line MZI sensor head based on inner air-cavity, a number of device samples of different sizes have been investigated and their transmission spectra, the corresponding spatial frequency spectra obtained by use of fast Fourier transform, and their microscope images are displayed in Fig. 3. It can be seen from Fig. 3 that the insertion loss of the tapered MZI is roughly ranged from 20 to 30 dB. Before the tapering process, the insertion loss of this device is ~5dB. When the diameter of the sensor head is relatively large (such as 95 $\mu$m), only one dominant side peak is located in the spatial frequency spectrum and the smooth fringe pattern in the transmission spectrum can be observed, due to the interference between the air-cavity mode and the silica-wall mode. When the sensor head diameter is gradually reduced, more side peaks exist in the spatial frequency spectrum and the spectral fringe pattern experiences more fluctuations. Finally, when the sensor head diameter is close to 20 $\mu$m, many side peaks appear in the spatial frequency spectrum and the interferometer is in multi-mode operation,

which involves the interference among the air-cavity mode and different silica-wall modes. Hence, more than one set of interference patterns can be observed in the transmission spectra of the second and the fourth samples. As shown in Fig. 3, the spatial frequency spectrum of the second sample has two relatively large side peaks while that of the fourth samples has many, but non-dominant side peaks, which makes some set of the fringe patterns of the latter has only poor fringe visibility and hardly to determine its FSR.

To test the system response to the RI change, the device sample was immersed into a series of RI liquids (from Cargille Laboratories) and the transmission spectra recorded had a resolution of 0.1 nm. Each time after the liquid sample was measured, the fiber sensor head was rinsed with methanol carefully until the original spectrum (i.e., the reference spectrum) could be restored and no residue liquid was left on the sensor head surface. The wavelength shifts of the two MZI sensor head samples with diameter of 95 and 60 $\mu$m, respectively, corresponding to different RI values, were plotted in Fig. 4(a) and (b), respectively. After implementing linear fit to the experimental data, the sensitivities obtained were 70 and 110 nm/RIU, respectively. The transmission spectra of the two samples, corresponding to a number of RI values, are shown in the insets of Fig. 4(a) and (b), where a red shift of the dip wavelength can be observed.

The dip wavelength shift with the RI change can be derived from (2) as

$$\delta\lambda_{\mathrm{dip}} = \frac{2L\delta n}{2m+1} \tag{4}$$

where $\delta n$ denotes the change in the effective RI of silica wall mode. As indicated by Eq. (4), the dip wavelength shift, and hence, the RI sensitivity could be enhanced by reducing the sensor head diameter, equivalent to thinning the silica wall or increasing the air-cavity (sensor head) length. Such a fact also becomes clear from the results shown in Fig. 4(a) and (b), respectively. When the diameter of the sensor head is too small (such as 20 $\mu$m), the interferometer device produces a multimode fringe pattern, which is highly sensitive to the external RI, however, the range of monotonic wavelength shift is only small. Moreover, the robustness of device is also reduced. We have also tested the RI response of a device sample with sensor head diameter of 20 $\mu$m and length of 4 mm, and the results obtained are recorded in Fig. 4(c), where an extremely high sensitivity of ~4202 nm/RIU is achieved, superior to most of the RI sensors reported [25], [26]. However, the RI measurement range is small, between 1.3241 and 1.3280. The measurement was implemented by immersing the sensor head into the RI liquid with value of 1.33 at room temperature (with the temperature coefficient of $3.37 \times 10^{-4}$/°C), and changing the liquid RI value by varying its temperature.

The high temperature sensing capability of the sensor was investigated by use of a tube furnace (CARBOLITE MTF 12/38/250). During the experiment, the sample was first heated to 1000 °C and maintained there for 2 h to remove the burnt fiber coating induced effects, and then, cooled down to room temperature. Next, the temperature was gradually increased to 100 °C, and then, to 1100 °C with a step of 100 °C, and stayed

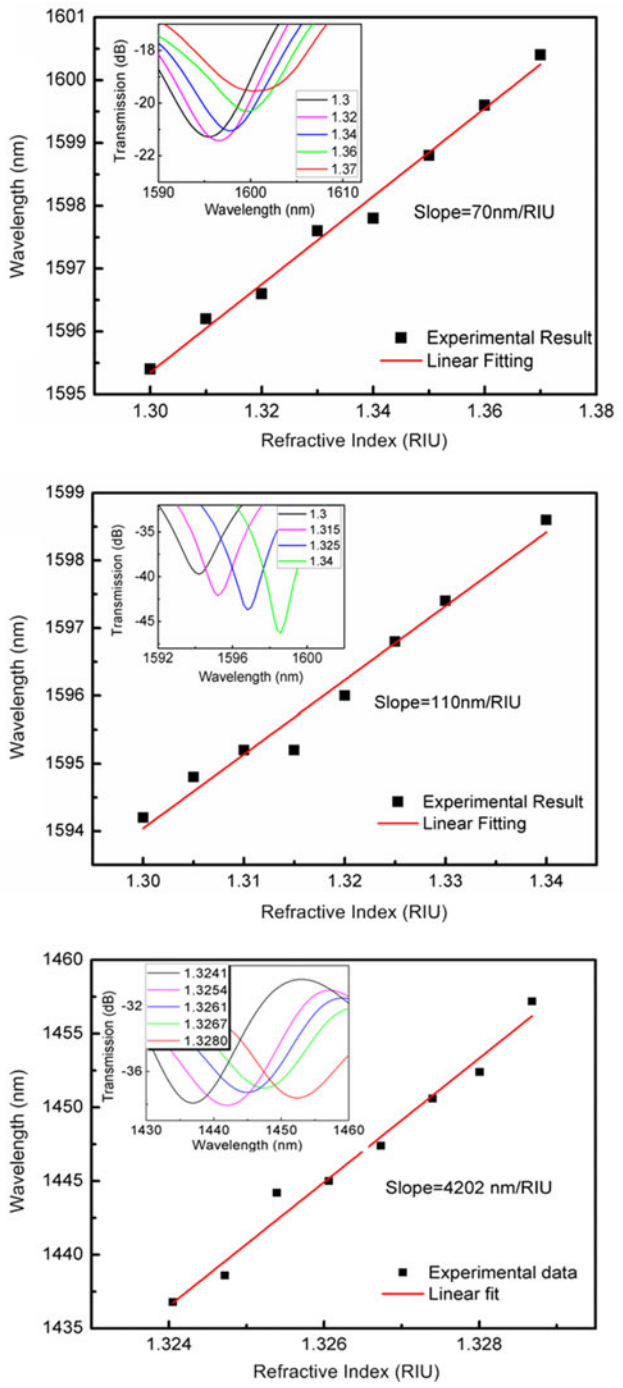


Fig. 4. (Color online) The dip wavelength shift with RI, and the insets show the transmission spectra of the device sample. (a) Sample with diameter of 95 $\mu$m. (b) Sample with diameter of 60 $\mu$m. (c) Sample with diameter of 20 $\mu$m.

for half an hour at each step. The device was kept at 1100 °C for 2 h before being cooling down, following the same steps as that in the heating process. The sample used in the high temperature test has a sensor head diameter of ~95 $\mu$m, the same as that used in the RI test. Fig. 5 presents the dip wavelength variation with the temperature change and its inset demonstrates the transmission spectra at different temperatures. An offset of 10 dB is artificially introduced for every 200 °C in the vertical

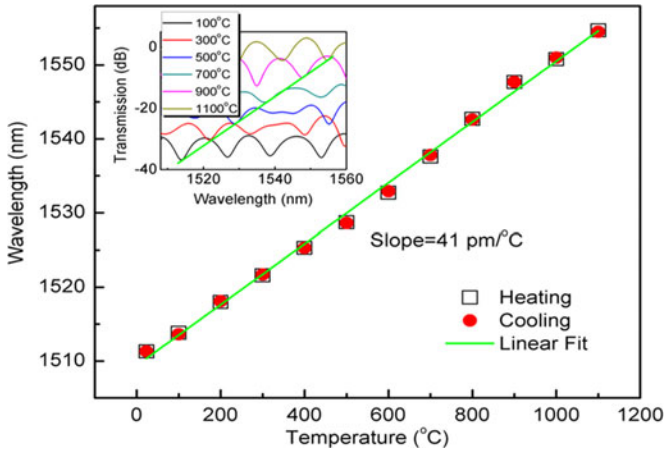


Fig. 5. The dip wavelength shift with temperature. The insets show the transmission spectra of the device sample at different temperatures. The device sample diameter is ~95 $\mu$m.

axis to observe the dip shift more clearly; however, the insertion loss of this device is hardly changed in the whole temperature test. A fringe dip at ~1510 nm at room temperature was found to experience a red shift with the increase of temperature. It can be seen from Fig. 5 that a good repeatability in both heating and cooling processes and a sensitivity of 41 pm/°C is achieved. Such temperature sensitivity is similar with those of the previously reported air-cavity based fiber MZIs [8], [13], [15]. From Eq. (2), the wavelength shift due to temperature increase can be expressed as

$$\delta\lambda_{\mathrm{dip}} = \frac{2(L+\delta L_T)(\Delta n+\delta n_T)}{2m+1} - \frac{2L\Delta n}{2m+1} \approx \frac{2(\Delta n\delta L_T + L\delta n_T)}{2m+1} \quad (5)$$

where $\delta L_T$ is the change of inner cavity length induced by material thermal-expansion and $\delta n_{\mathrm{T}}$ denotes the change in effective RI of the silica wall mode, due to thermal-optical effect. The thermal-optical effect plays the dominant role as the thermo-optic coefficient ($7.8 \times 10^{-6}$) in silica is larger than thermal expansion coefficient ($4.1 \times 10^{-7}$).

Taking the sample with the RI sensitivity of 4202 nm/RIU in Fig. 4(c) as an example, if no temperature compensation is employed, the RI measurement error resulting from temperature cross sensitivity is $\sim 9.8 \times 10^{-6}$ RIU/ °C, which should be considered in practical measurement.

## V. Conclusion

By fabricating an air-cavity inside the microfiber, an ultra compact optical fiber MZI sensor head can be created, in which the fascinating features of microfiber are efficiently combined with the highly sensitive MZI and the sensitivities achieved for RI and temperature are ~4202 nm/RIU and 41 pm/ °C, respectively, with excellent high temperature sustainability up to 1100 °C. The device developed is a promising candidate for many chemical and biological sensing and environmental monitoring applications.

## References

[1] Y. J. Rao, M. Deng, D. W. Duan, X. C. Yang, T. Zhu, and G. H. Cheng, "Micro Fabry-Perot interferometers in silica fibers machined by femtosecond laser," *Opt. Exp.*, vol. 15, pp. 14123–14128, 2007.
[2] T. Wei, Y. Han, H. L. Tsai, and H. Xiao, "Miniaturized fiber inline Fabry-Perot interferometer fabricated with a femtosecond laser," *Opt. Lett.*, vol. 33, pp. 536–538, 2008.
[3] D. W. Kim, Y. Zhang, K. L. Cooper, and A. Wang, "In-fiber reflection mode interferometer based on a long-period grating for external refractive-index measurement," *Appl. Opt.*, vol. 16, pp. 1387–1389, 2008.
[4] Z. B. Tian, S. S. H. Yam, and H.-P. Loock, "Single-mode fiber refractive index sensor based on core-offset attenuators," *IEEE Photon. Technol. Lett.*, vol. 20, no. 16, pp. 1387–1389, Aug. 2008.
[5] C. R. Liao, T. Y. Hu, and D. N. Wang, "Optical fiber Fabry-Perot interferometer cavity fabricated by femtosecond laser micromachining and fusion splicing for refractive index sensing," *Opt. Exp.*, vol. 20, pp. 22813–22818, 2012.
[6] L. Yuan, J. Yang, and Z. Liu, "A compact fiber-optic flow velocity sensor based on a twin-core fiber Michelson interferometer," *IEEE Sensors J.*, vol. 8, no. 7, pp. 1114–1117, Jul. 2008.
[7] C. R. Liao, D. N. Wang, M. Wang, and M. H. Yang, "Fiber in-line Michelson interferometer tip sensor fabricated by femtosecond laser," *IEEE Photon. Technol. Lett.*, vol. 24, no. 22, pp. 2060–2063, Nov. 2012.
[8] J. H. Lim, H. S. Jang, K. S. Lee, J. C. Kim, and B. H. Lee, "Mach-Zehnder interferometer formed in a photonic crystal fiber based on a pair of long-period fiber gratings," *Opt. Lett.*, vol. 29, pp. 346–348, 2004
[9] J. Villatoro, V. P. Minkovich, and D. Monzón-Hernández, "Compact modal interferometer built with tapered microstructured optical fiber," *IEEE Photon. Technol. Lett.*, vol. 18, no. 11, pp. 1258–1260, Jun. 2006
[10] P. Lu, L. Men, K. Sooley, and Q. Chen, "Tapered fiber Mach–Zehnder interferometer for simultaneous measurement of refractive index and temperature," *Appl. Phys. Lett.*, vol. 94, p. 131110, 2009.
[11] L. V. Ngyuen, D. Hwang, S. Moon, D. S. Moon, and Y. J. Chung, "High temperature fiber sensor with high sensitivity based on core diameter mismatch," *Opt. Exp.*, vol. 16, pp. 11369–11375, 2008.
[12] Y. Jung, S. Lee, B. H. Lee, and K. Oh, "Ultracompact in-line broadband Mach-Zehnder interferometer using a composite leaky hollow-optical-fiber waveguide," *Opt. Lett.*, vol. 33, pp. 2934–2936, 2008.
[13] M. Park, S. Lee, W. Ha, D. K. Kim, W. Shin, I. B. Sohn, and K. Oh, "Ultracompact intrinsic micro air-cavity fiber Mach-Zehnder interferometer," *IEEE Photon. Technol. Lett.*, vol. 21, no. 15, pp. 1027–1029, Aug. 2009.
[14] J. Villatoro, V. Finazzi, G. Coviello, and V. Pruneri, "Photonic-crystal-fiber enabled micro-Fabry-Perot interferometer," *Opt. Lett.*, vol. 34, pp. 2441–2443, 2009.
[15] Y. Wang, Y. Li, C. Liao, D. N. Wang, M. Yang, and P. Lu, "High-temperature sensing using miniaturized fiber in-line Mach–Zehnder interferometer," *IEEE Photon. Technol. Lett.*, vol. 22, no. 1, pp. 39–41, Jan. 2010.
[16] Y. Wang, M. W. Yang, D. N. Wang, S. J. Liu, and P. X. Lu, "Fiber in-line Mach–Zehnder interferometer fabricated by femtosecond laser micromachining for refractive index measurement with high sensitivity," *J. Opt. Soc. Amer. B*, vol. 27, pp. 370–374, 2010.
[17] C. L. Lee, H. J. Chang, Y. W. You, G. H. Chen, J. M. Hsu, and J. S. Horng, "Fiber Fabry-Perot interferometers based on air-bubbles/liquid in hollow core fibers," *IEEE Photon. Technol. Lett.*, vol. 26, no. 8, pp. 749–752, Apr. 2014.
[18] S. Liu, Y. P. Wang, C. R. Liao, G. J. Wang, Z. Y. Li, Q. Wang, J. T. Zhou, K. M. Yang, X. Y. Zhong, J. Zhao, and J. Tang, "High-sensitivity strain sensor based on in-fiber improved Fabry-Perot interferometer," *Opt. Lett.*, vol. 39, pp. 2121–2124, 2014.
[19] C. R. Liao, S. Liu, L. Xu, C. Wang, Y. P. Wang, Z. Y. Li, Q. Wang, and D. N. Wang, "Sub micron silica diaphragm-based fiber-tip Fabry–Perot interferometer for pressure measurement," *Opt. Lett.*, vol. 39, pp. 2827–2830, 2014.
[20] L. Tong, R. R. Grattass, J. B. Ashcom, S. He, J. Lou, M. Shen, I. Maxwell, and E. Mazur, "Subwavelength-diameter sclica wires for low-loss optical wave guiding," *Nature*, vol. 426, pp. 816–819, 2003.
[21] G. Brambilla, V. Finazzi, and D. J. Richardson, "Ultra-low-loss optical fiber nanotapers," *Opt. Exp.*, vol. 12, pp. 2258–2263, 2004.

[22] P. Polynkin, A. Polynkin, N. Peyghambarian, and M. Mansuripur, "Evanescent field-based optical fiber sensing device for measuring the refractive index of liquids in microfluidic channels," *Opt. Lett.*, vol. 30, pp. 1273–1275, 2005.
[23] X. Fang, C. R. Liao, and D. N. Wang, "Femtosecond laser fabricated fiber Bragg grating in microfiber for refractive index sensing," *Opt. Lett.*, vol. 35, pp. 1007–1009, 2010.
[24] C. R. Liao, D. N. Wang, and Y. Wang, "Microfiber in-line Mach-Zehnder interferometer for strain sensing," *Opt. Lett.*, vol. 38, pp. 757–759, 2013.
[25] X. Fan, I. M. White, S. I. Shopova, H. Zhu, J. D. Suter, and Y. Sun, "Sensitive optical biosensors for unlabeled targets: A review," *Analytical Chimica Acta*, vol. 620, pp. 8–26, 2008.
[26] A. N. Chryssis, S. M. Lee, S. B. Lee, S. S. Saini, and M. Dagenais, "High sensitivity evanescent field fiber bragg grating sensor," *IEEE Photon. Technol. Lett.*, vol. 17, no. 6, pp. 1253–1255, Jun. 2005.

**C. R. Liao** received the B.E. degree in optical information science and technology and the M. S. degree in physical electronics from the Huazhong University of Science and Technology, Wuhan China, in 2005 and 2007, respectively, and the Ph.D degree in electrical engineering from The Hong Kong Polytechnic University, Hong Kong, in 2012. He is currently an Assistant Professor in Shenzhen University, China. His current research interest include optical fiber sensor and femtosecond laser micromachining.

**H. F. Chen** received the B. Sc. degree in optical electronics information engineering, the M. Sc. degree in optical engineering, both from Zhejiang University, Hangzhou, China, in 2001 and 2004, respectively, where she is also currently working toward the Ph. D. degree. Her main research interests include femtosecond laser micromachining, optical fiber communications, and optical fiber sensors.

**D. N. Wang** received the B.Sc. degree in telecommunications from the Beijing University of Posts and Telecommunications, China, in 1982, the MBA degree from the University of Ulster, U. K., in 1989, and the Ph.D. degree from City University, London, U.K. in 1995.

His main research interests include ultrafast optics, femtosecond laser micromachining, fiber laser, optical fiber communications, and optical fiber sensors. He has more than 150 international journal publications.